



OPEN

# Dual beam and dual circular polarized multiplexing reflectarray for Ku band satellite communication

Yutian Ma<sup>1</sup>, Yuhui Ren<sup>1</sup>✉, Lehu Wen<sup>2</sup>, Rongli Zhao<sup>1</sup>, Ke Li<sup>1</sup>, Fuwei Wang<sup>1</sup>, Feng Cui<sup>3</sup> & Handong Wu<sup>3</sup>

In this letter, a broadband low-profile dual circularly polarized reflectarray (dual-CP RA) for Ku-band satellite communications is proposed. A novel single-layer metasurface unit cell consisting of a functional layer, an air layer and a metal plate is investigated first. The functional layer is a metal structure printed on the F4B substrate. The air layer can effectively extend the bandwidth, and the overall profile is only  $0.12\lambda_0$ , where  $\lambda_0$  represents the wavelength at 11.725 GHz. To independently control the phase of left-handed circularly polarized (LHCP) and right-handed circularly polarized (RHCP) waves, Dynamic phase and Berry phase methods are employed by either changing the size of microstrip lines or the rotating of the cells. Finally, a dual-CP RA with 1600 cells is designed to realize two beams at  $20^\circ$  for LHCP wave and  $-20^\circ$  for RHCP wave at 11.725 GHz. The measured gain for LHCP wave is 29.1 dB with the aperture efficiency (AE) of 47% and 1-dB gain bandwidth of 37.4%, while the gain, AE, and bandwidth for RHCP wave are 29.22 dB, 48.3% and 37% respectively.

**Keywords** Reflectarray, Dual-circular polarization, Low profile

In satellite communication, radar, and other applications requiring long-distance signal transmission, the gain of antenna is undoubtedly one of the most critical indicators. Compared with the conventional high-gain antennas, such as the phased array, the reflector antenna, etc., the reflectarray (RA) based on the metasurface can independently control the amplitude, phase, polarization and other characteristics of electromagnetic waves. In the past few years, the work on RA has primarily focused on achieving high-gain radiation in single or multi-frequency bands<sup>1–3</sup>. Recently, RA with polarization multiplexing performance in multi-frequency and broadband has gradually become a new focus to improve the efficiency of spectrum utilization. In particular, dual circularly polarized (dual-CP) RA that can radiate LHCP and RHCP waves in different channels can greatly improve the data transmission rate and reduce the polarization loss.

As shown in Fig. 1, the dual-CP RA is mainly composed of two parts: the feed and reflector. The feed is generally a horn antenna, and the reflector is a metasurface composed of periodic unit cells. Dual-CP RA can achieve reflection with the same polarization. When an LHCP wave is incident, a high-gain LHCP reflected wave with a directional angle of  $(\phi L, \theta L)$  is generated. When a RHCP wave is incident, the direction of RHCP reflected wave is  $(\phi R, \theta R)$ . In order to reflect the LHCP and RHCP waves in different directions, each cell is required to have a different phase compensation for the LHCP and RHCP waves, respectively.

The first method to realize dual-CP RA is to combine the LHCP and RHCP reflector, and adopt a double-layer or even multi-layer structure to achieve dual-CP RA<sup>4,5</sup>. But the multi-layer structure has the disadvantages of large loss, low efficiency, and narrow band width (BW).

In the second method, the reflective metasurfaces with polarization conversion function can be designed to convert linearly polarized (LP) waves into CP waves. In Ref.<sup>6</sup>, a wideband dual-LP RA is designed, and integrated it with a polarizer to obtain independent dual-CP beams. However, this type of RA is also generally multi-layered.

The third method is to realize dual-CP RA by using both Dynamic phase (DP) and Berry phase (BP)<sup>7–14</sup>. Specifically, the DP is regulated by changing the size of cells, and the incident CP waves are reflected with the same handedness. Then the cells are rotated to regulate the BP, separating the LHCP and RHCP reflections

<sup>1</sup>School of Information Science and Technology, Northwest University, Xi'an 710127, China. <sup>2</sup>Department of Electronic and Electrical Engineering, Brunel University London, Uxbridge UB8 3PH, UK. <sup>3</sup>Xi'an HengDa Microwave Technology Development Co., Ltd, Xi'an, China. ✉email: ryhui@nwu.edu.cn

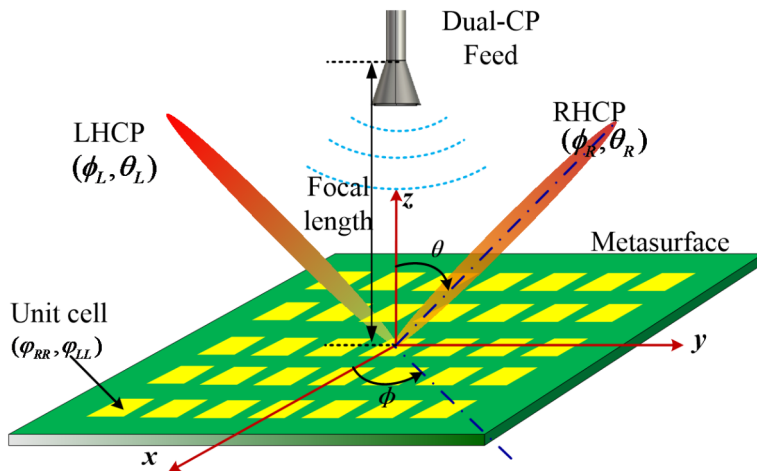


**Fig. 1.** Diagram of dual-CP RA. Each RA cell imposes an independent phase delay of  $\varphi_{RR}$  and  $\varphi_{LL}$  for RHCP and LHCP waves, respectively.

in different channels. In Ref.<sup>7</sup>, two sets of orthogonally placed printed dipoles are designed on a double-layer substrate. By adjusting BP and DP, the LHCP and RHCP reflected beams are controlled independently. In Refs.<sup>8,9</sup>, Z.H. Jiang's team designed two unit cells of dual-CP RA using multi-layer metal and dielectric. These designs also integrates BP and DP to control the LHCP and RHCP reflected beams. In Ref.<sup>10</sup>, a dual-CP RA with the advantages of low-profile and wide band is proposed. The cell is composed of an elliptical ring, arc-shaped and rectangular metal microstrip lines, and there is only one dielectric substrate. The works in<sup>11–13</sup> is similar to that of Ref.<sup>10</sup>, which all use a single layer substrate. A new idea of dual-CP RA is introduced in<sup>14</sup>, which uses a single-fed CP antenna as the cell of the RA. The received RHCP wave is adjusted by DP, while the LHCP wave is controlled by BP.

In this letter, a novel dual-CP RA covering Ku-band satellite communication downlink band (10.7–12.75 GHz) is proposed. First of all, unlike the previous dual-CP RA, it radiates LHCP and RHCP waves in different bands. The RA proposed in the letter realizes dual-CP multiplexing in the same band, which can greatly improve the spectrum utilization efficiency. Secondly, BP and DP are used to excite and separate the dual-CP beam in our work. Compared with the similar works in the existing literatures, the presented structure uses only one layer of dielectric substrate, and the unit cell is simpler. However, the performance of the antenna has been greatly improved, especially under the premise that the aperture efficiency (AE) is almost unchanged, the profile and bandwidth of the antenna have been significantly improved.

## Design of dual-CP cells

### Basic theories and design methods

It is possible to independently regulate phase compensation ( $\varphi_{LL}$  and  $\varphi_{RR}$ ) by using DP and BP, as shown in Fig. 2. BP compensation is implemented by rotating the unit cell. Suppose the rotation angle of the cell is  $\varphi_r$ , then  $\varphi_{LL}$  and  $\varphi_{RR}$  have opposite symbols<sup>15</sup>, i.e.

$$\varphi_{LL} = -2\varphi_r, \varphi_{RR} = 2\varphi_r \quad (1)$$

Thus, when  $\varphi_r$  varies a linear gradient, the LHCP and RHCP reflected waves point in two symmetric directions, that is,  $\theta_R = -\theta_L$ . DP compensation is achieved by changing the size of cells. If the reflector is composed of isotropic cells, it provides the same phase compensation  $\varphi_d$  for the LHCP and RHCP waves<sup>10</sup>. Therefore, both the LHCP and RHCP reflected waves propagate in the same direction,  $\theta_R = \theta_L$ . In summary, if the DP and BP are combined, LHCP and RHCP waves can be independently regulated. And satisfied:

$$\varphi_{LL} = \varphi_d - 2\varphi_r, \quad \varphi_{RR} = \varphi_d + 2\varphi_r \quad (2)$$

The reflection coefficient ( $\Gamma$ ) of the dual-CP cells are investigated by the CST software. Assuming that a LP incident waves can be decomposed into a horizontal component and a vertical component, the  $\Gamma$  matrix is expressed as<sup>16</sup>:

$$\Gamma = \begin{bmatrix} \Gamma_{HH} & \Gamma_{HV} \\ \Gamma_{VH} & \Gamma_{VV} \end{bmatrix} \quad (3)$$

Then, the  $\Gamma$  of CP incident waves can be numerically derived from (3):

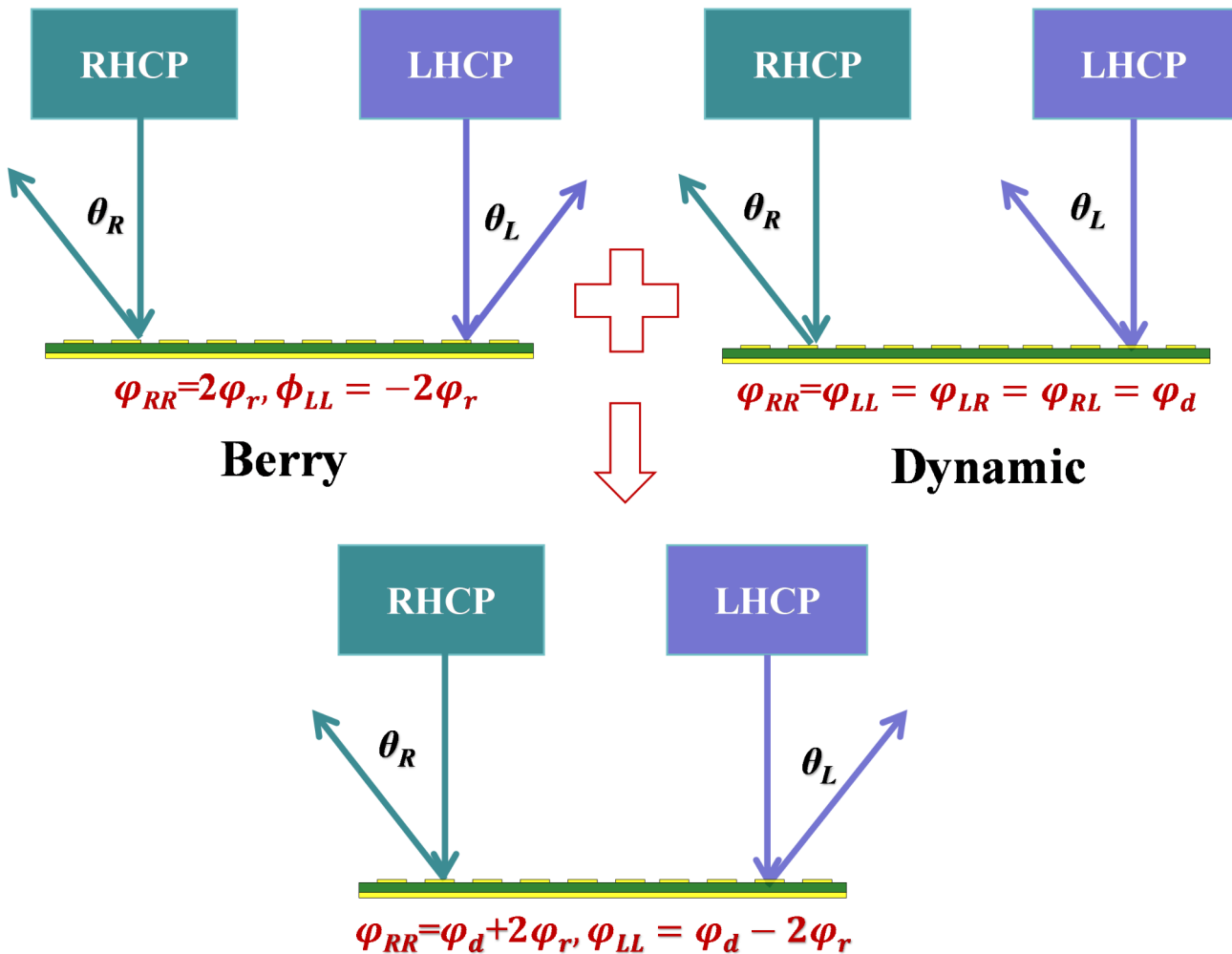


**Fig. 2.** Illustration of the intuitive concept of combining BP and DP for achieving independent dual-CP phase compensation.

$$\begin{aligned}
 \Gamma_{RR} &= [(\Gamma_{HH} - \Gamma_{VV}) + j(\Gamma_{HV} + \Gamma_{VH})]e^{j2a}/2 \\
 \Gamma_{LL} &= [(\Gamma_{HH} - \Gamma_{VV}) - j(\Gamma_{HV} + \Gamma_{VH})]e^{j2a}/2 \\
 \Gamma_{LR} &= [(\Gamma_{HH} + \Gamma_{VV}) + j(\Gamma_{HV} - \Gamma_{VH})]e^{j2a}/2 \\
 \Gamma_{RL} &= [(\Gamma_{HH} + \Gamma_{VV}) - j(\Gamma_{HV} - \Gamma_{VH})]e^{j2a}/2
 \end{aligned} \tag{4}$$

In these formulas,  $\Gamma_{HH}$ ,  $\Gamma_{VV}$ ,  $\Gamma_{LL}$  and  $\Gamma_{RR}$  denote the co-polarization reflection coefficients, and  $\Gamma_{HV}$ ,  $\Gamma_{VH}$ ,  $\Gamma_{LR}$  and  $\Gamma_{RL}$  denote the cross-polarization reflection coefficients. In general, the unit cells need to meet three conditions to realize dual-CP RA<sup>10</sup>: (1) The reflection phase of the two components of the LP incident wave has a phase difference of 180°, that is, (1)  $\varphi(\Gamma_{HH}) - \varphi(\Gamma_{VV}) = 180^\circ$ . (2) The phase compensation in 0°–360° can be achieved by adjusting the DP. (3) The BP can be changed by rotating the cells.

#### Design of the unit cell

Figure 3 shows the unit cell of the proposed dual-CP RA, which consists of a functional layer, an air layer and a metal plate. The functional layer is a metal structure printed on the F4B ( $\epsilon_r = 2.2$ ,  $\tan\delta = 0.001$ ) substrate with a thickness  $h_1$ , consisting of a hexagonal split ring (HSR) and a smaller hexagonal patch concentrically placed. The HSR is a bent phase delay line with a length of  $l = (3l_1/2 + l_2 + l_3) * 2$ , and a width of  $w_1$ . With the change of  $l$ , the DP also changes. At the same time, the operating frequency of the cell will be shifted. Fortunately, the shift can be corrected by the hexagonal patch with a side length  $l_4$ . The effect of the air layer is to extend the bandwidth of the unit, and its thickness is  $h_2$ . The overall height of the RA ( $h_1 + h_2$ ) is about  $0.12\lambda_0$ , where  $\lambda_0$  represents the wavelength at 11.725 GHz.

#### Dynamic phase control

Arbitrary DP compensation in the 0°–360° range can be achieved by controlling the parameters  $l$ ,  $l_4$  and  $w_1$ . For the sake of simplicity, two states are set in this design. In state 1, the rotation angle of each cell (No. 1–18) is 0°.

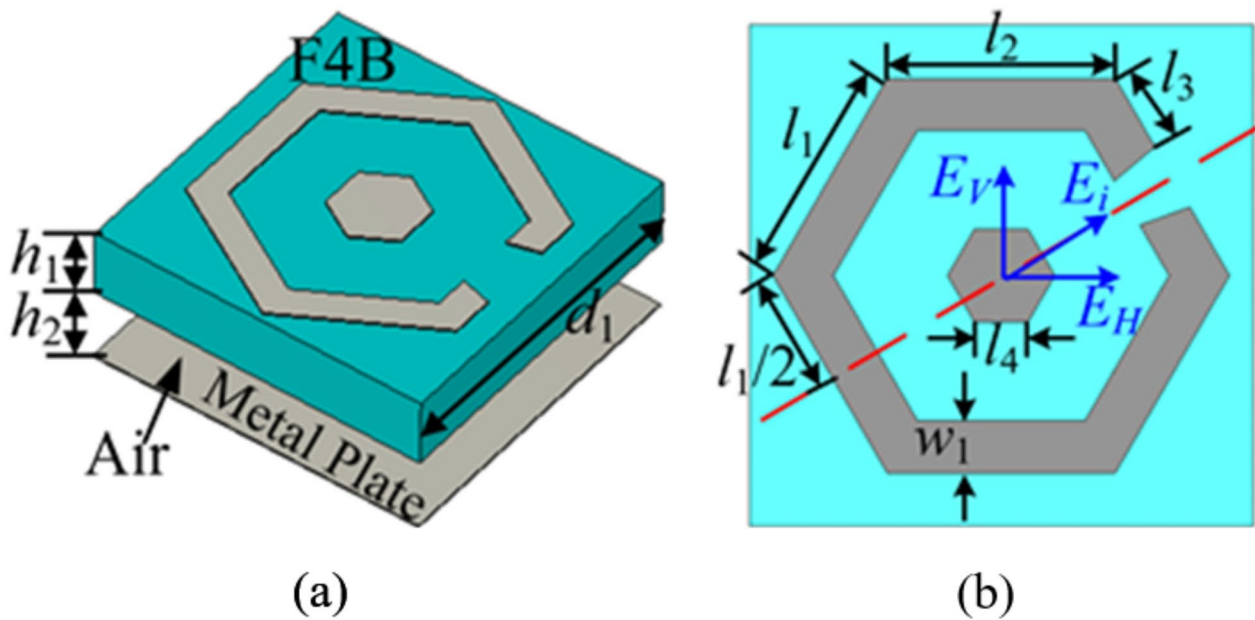


**Fig. 3.** (a) 3-D view of the dual-CP RA element. (b) Planar views of top layer. The dimensions are  $l_1 = l_2 = 3.4$ ,  $h_1 = 1.5$ ,  $d_1 = 7.5$ , and  $h_2 = 1.6$ , all in millimeters.

No.	1/19	2/20	3/21	4/22	5/23	6/24	7/25	8/26	9/27
DP/o	0/180	10/190	20/200	30/210	40/220	50/230	60/240	70/250	80/260
$l$	11.8	12.9	14	14.5	14.6	15.1	15.7	17	17.4
$w_1$	1.4	1.2	1.2	1.3	1.2	1.2	1.2	1.5	1.5
$l_4$	0.2	1	1	1	1.8	1.8	1.8	1	1
No.	10/28	11/29	12/30	13/31	14/32	15/33	16/34	17/35	18/36
DP/o	90/270	100/280	110/290	120/300	130/310	140/320	150/330	160/340	170/350
$l$	17.6	18.5	18.5	19.2	19.3	19.5	19.6	19.9	20.2
$w_1$	1.5	1.4	1.2	0.96	0.74	0.55	0.37	0.27	0.18
$l_4$	1	1.5	1.5	1.5	1.5	1.5	2	1.5	2

**Table 1.** Parameters of RA cells (mm).

Every cells with different sizes cover the DP from  $0^\circ$  to  $170^\circ$ , that is, the step of phase change is  $10^\circ$ . Then, rotate all the cells by  $90^\circ$  to get state 2. Another 18 cells (No. 19–36) then cover a range of  $180^\circ$  to  $350^\circ$ . The dimensions of the 36 cells are shown in Table 1. Since the difference between state 2 and 1 is only in rotation angle, the 18 cells of state 1 will be taken as an example for simulation. First, the incident wave is assumed to be LP. Figure 4 shows the  $\Gamma$  of each cell, including amplitude and phase. As shown in Fig. 4a–c, the  $|\Gamma_{HH}|$  and  $|\Gamma_{VV}|$  are greater than  $-0.05$  dB, and the  $|\Gamma_{HV}|$  and  $|\Gamma_{VH}|$  are less than  $-50$  dB from  $8.5$  GHz to  $15$  GHz. Because HSR and the hexagonal patch both are symmetrical structures,  $|\Gamma_{VH}|$  and  $|\Gamma_{HV}|$  are equal. It indicates that the incident wave is almost completely reflected with high purity by the proposed unit cell. From Fig. 4d–f, it can be seen that the phase difference of the  $\Gamma_{HH}$  and  $\Gamma_{VV}$  is about  $180^\circ$  in a wider band. The result satisfies the first condition.

Then, the  $\Gamma$  of the CP incident wave is calculated by formula (4).  $\Gamma_{HV}$  and  $\Gamma_{VH}$  are ignored, so there are  $\Gamma_{LL} = \Gamma_{RR}$  and  $\Gamma_{LR} = \Gamma_{RL}$ . As shown in Fig. 5a, b, the  $|\Gamma_{LL}|$  and  $|\Gamma_{RR}|$  are greater than  $-0.5$  dB,  $|\Gamma_{LR}|$  and  $|\Gamma_{RL}|$  are less than  $-10$  dB from  $8.5$  GHz to  $15$  GHz. This indicates that each cell can reflect both LHCP and RHCP incident waves with high efficiency and the same handedness. Figure 5c, d shows that the reflection phase of each cell changes approximately linearly.

When  $f = 11.725$  GHz, the reflection phase for cell 1 is  $30.65^\circ$ , and for cell 18 is  $-140.01^\circ$ . Obviously, the 18 cells in state 1 can perform DP compensation in the range of  $0^\circ$ – $180^\circ$ . Combined with state 2, DP compensation in the  $360^\circ$  range can be basically achieved. It is that meets the second condition.

#### Berry phase control

Figure 6 shows the relationship between the reflection phase of the co-polarized CP wave and rotation angle of the cells at different frequencies. When the angle gradually changes from  $-90^\circ$  to  $90^\circ$ , reflection phase presents a precisely linear increase or decrease, and can cover a range from  $0^\circ$  to  $360^\circ$ . Specifically, when the cell is rotated  $1^\circ$  counterclockwise, the reflected phase of the LHCP wave decreases by  $2^\circ$  and that of the RHCP wave increases

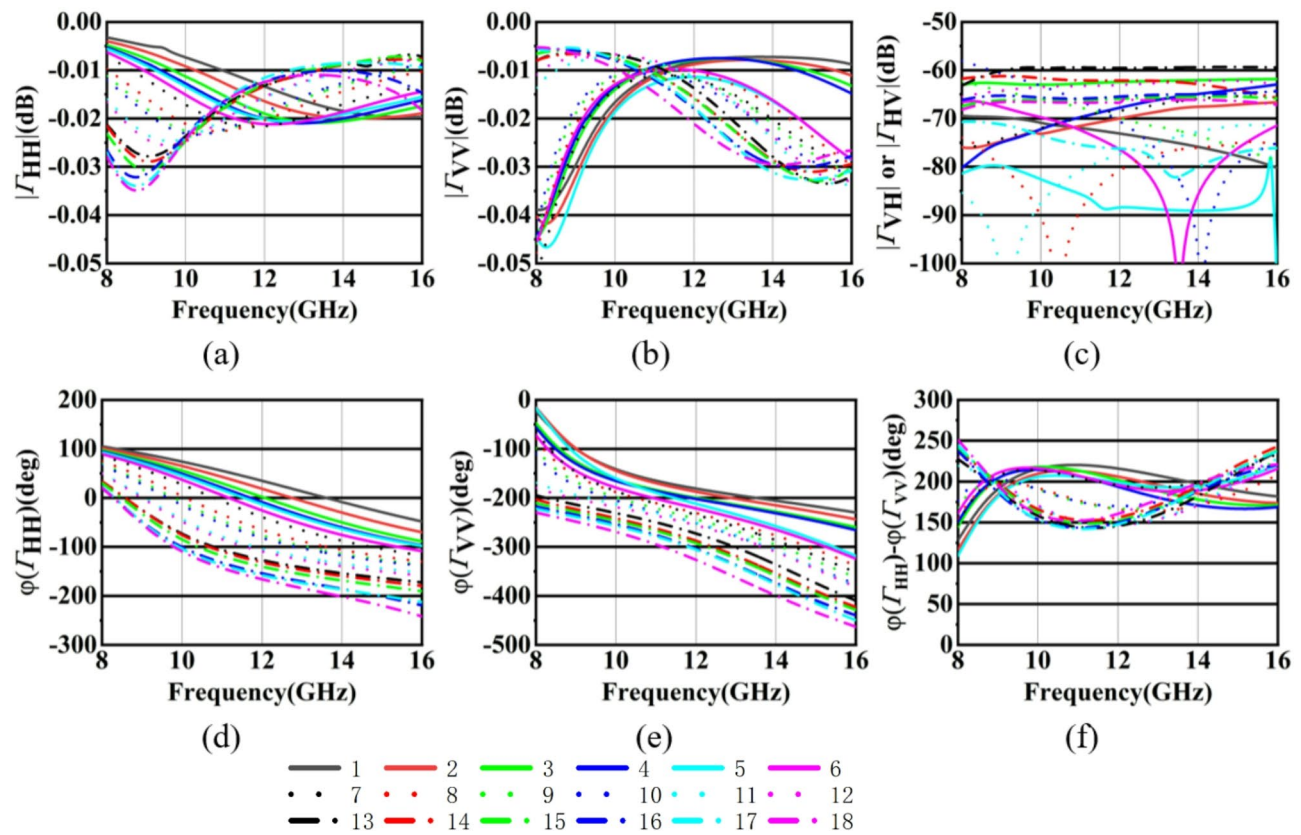


**Fig. 4.** The simulated  $\Gamma$  of LP wave by CST, (a)  $|\Gamma_{HH}|$ , (b)  $|\Gamma_{VV}|$ , (c)  $|\Gamma_{HV}|$  or  $|\Gamma_{VH}|$ , (d)  $\phi(\Gamma_{HH})$ , (e)  $\phi(\Gamma_{VV})$ , (f)  $\phi(\Gamma_{HH}) - \phi(\Gamma_{VV})$ .

by  $2^\circ$ . At this point, the third condition for dual-CP RA have been satisfied. The BP can be better called through the rotation of the cell.

#### Oblique incidence performance of the cells

In an array, the incoming wave from the feed source is not illuminated vertically for most units. Therefore, we first studied the wide incidence angle characteristics of the proposed unit cell, as shown in Fig. 7. Considering that the incident angle of the electromagnetic waves received by the edge-located units in the actual design is approximately  $30^\circ$ , the variation range of the oblique incidence angle is set from  $0^\circ$  to  $30^\circ$ . For simplicity, we selected cell No. 10 and simulated after rotating them by  $30^\circ$  and  $110^\circ$ , respectively. It can be seen that when the incidence Angle increases gradually from  $0^\circ$  to  $30^\circ$ , although the copolarization reflection coefficient decreases gradually, it can still maintain a high reflectivity ( $\Gamma > -0.5$  dB), and the cross-polarization reflection coefficient is less than  $-10$  dB. In addition, the reflection phase of the unit is almost unchanged in this angle range, indicating that the unit cells have a stable phase shift characteristic and can carry out more accurate phase compensation for the incident wave.

#### Array design and results

When composing the array with the proposed unit cells, the required phase shift for each cell needs to be calculated<sup>17</sup>, as follow:

$$\Theta = k_0 \cdot [d_i - (x_i \cos \phi + y_i \sin \phi) \sin \theta] \quad (5)$$

Referring to Fig. 1, the  $\Theta$  represents  $\varphi_{LL}$  or  $\varphi_{RR}$ ,  $(x_i, y_i)$  represents the position of each cell,  $d_i$  represents the distance between the feed and the cell, and  $(\phi, \theta)$  represents  $(\phi L, \theta L)$  or  $(\phi R, \theta R)$ . After obtaining  $\Theta$ , DP phase compensation or rotation angle can be obtained by formula (1) and (2). Further, it is possible to correspond DP to the sizes of the cell by Table 1. Using Fig. 6, BP can be mapped to the rotation angle of each cell. Finally, the cells are combined into an array with a size  $300 \text{ mm} \times 300 \text{ mm}$ . It is fed by a dual-CP horn with a diameter of 40 mm. The focal diameter ratio is 0.866, and the focal length is 259.8 mm. The desired direction of the two beams is  $(\phi L, \theta L) = (90^\circ, 20^\circ)$  and  $(\phi R, \theta R) = (-90^\circ, -20^\circ)$  respectively. The DP and rotation angle distribution of dual-CP RA cells are respectively shown in Fig. 8a, b.

To verify the performance of the designed dual-CP RA, a prototype was fabricated and tested (Fig. 9). Figure 10 shows the gain and axial ratio (AR) frequency response of the dual-CP RA. In the band of 8–16 GHz, the AR is less than 3 dB. The 1 dB gain bandwidth of the antenna is 37.4% (10.62–15.5 GHz) and 37% (10.68–15.53 GHz).

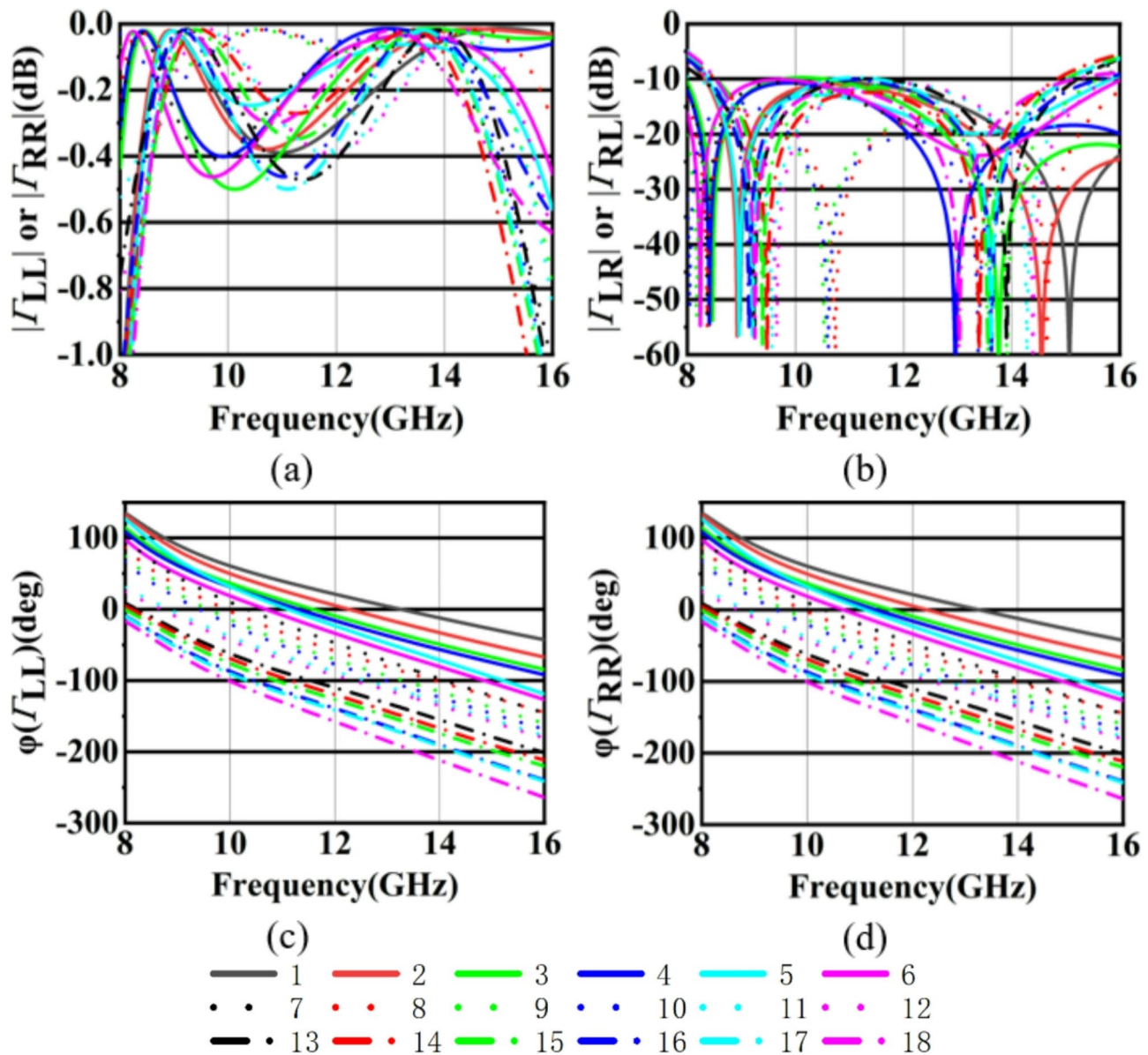


**Fig. 5.** The calculated  $\Gamma$  of CP incident wave obtained by formula (4), (a)  $|\Gamma_{LL}|$  or  $|\Gamma_{RR}|$ , (b)  $|\Gamma_{LR}|$  or  $|\Gamma_{RL}|$ , (c)  $\phi(\Gamma_{LL})$ , (d)  $\phi(\Gamma_{RR})$ .

when the LHCP and RHCP waves are incident respectively. Figure 11 shows the radiation patterns of the dual-CP RA. When a LHCP wave is incident, the reflected beam direction is  $(\phi_L, \theta_L) = (90^\circ, 20^\circ)$  with a peak gain of 29.1 dB and an AE of 47%. When a RHCP wave is incident, the direction is  $(\phi_R, \theta_R) = (-90^\circ, -20^\circ)$  with a gain of 29.2 dB and an AE of 48.3%. Moreover, the side lobe level and the cross-polarization levels of the antenna are both less than -15 dB. In general, the AR bandwidth, gain bandwidth and impedance bandwidth of the dual-CP RA almost cover the downlink band of Ku-band satellite communication.

Table 2 compares the performance of the developed RA with other recently reported works. As can be seen, compared with the design of the multifunctional layer<sup>5–8</sup> the structural complexity is greatly reduced, the array profile and weight are well controlled, meanwhile, the fabricating cost is effectively reduced. Compared with other RA designed with one substrate<sup>9</sup>, our work shows a better cross-polarization level, a wider 1 dB gain BW. Reference<sup>10</sup> has a similar BW of cell and gain BW to ours, but our work has a lower profile. For some application scenarios with stringent space requirements, a lower antenna array profile can better adapt to the limited installation space.

## Discussion

Firstly, in this letter, the theory, design, and experimental verification of low-profile and wideband dual-CP RA for Ku-band downlink satellite communication are reported. Using DP and BP compensation method, we can radiate LHCP and RHCP waves in any direction. The measured results confirmed that the LHCP beam of

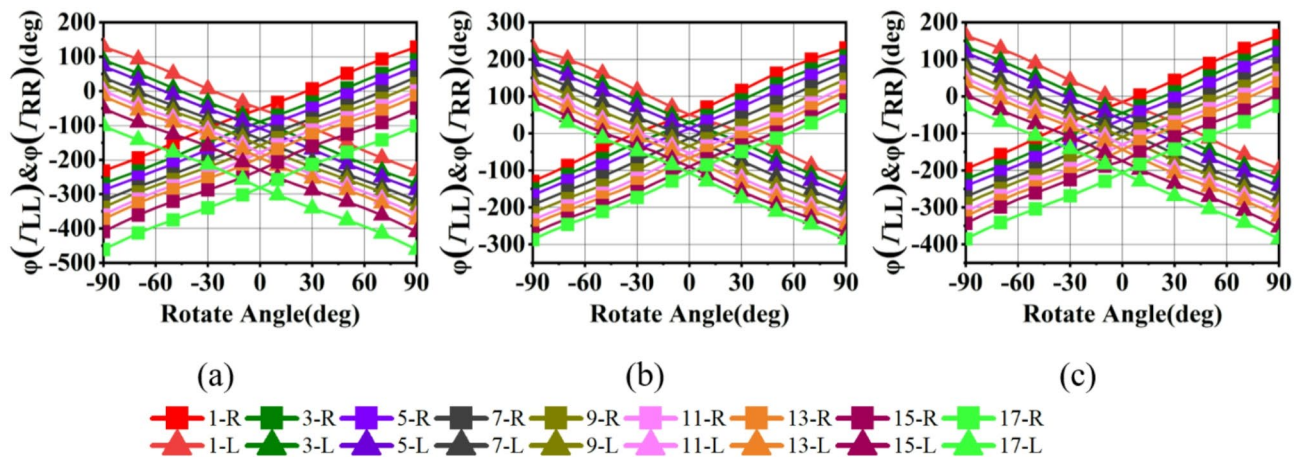


**Fig. 6.** The simulated co-polarized reflection phase change curve with cells rotation angle at (a) 8.5, (b) 11.725, and (c) 15 GHz. The rising curves represent  $\varphi(\Gamma_{RR})$  and the falling curve represents  $\varphi(\Gamma_{LL})$ .

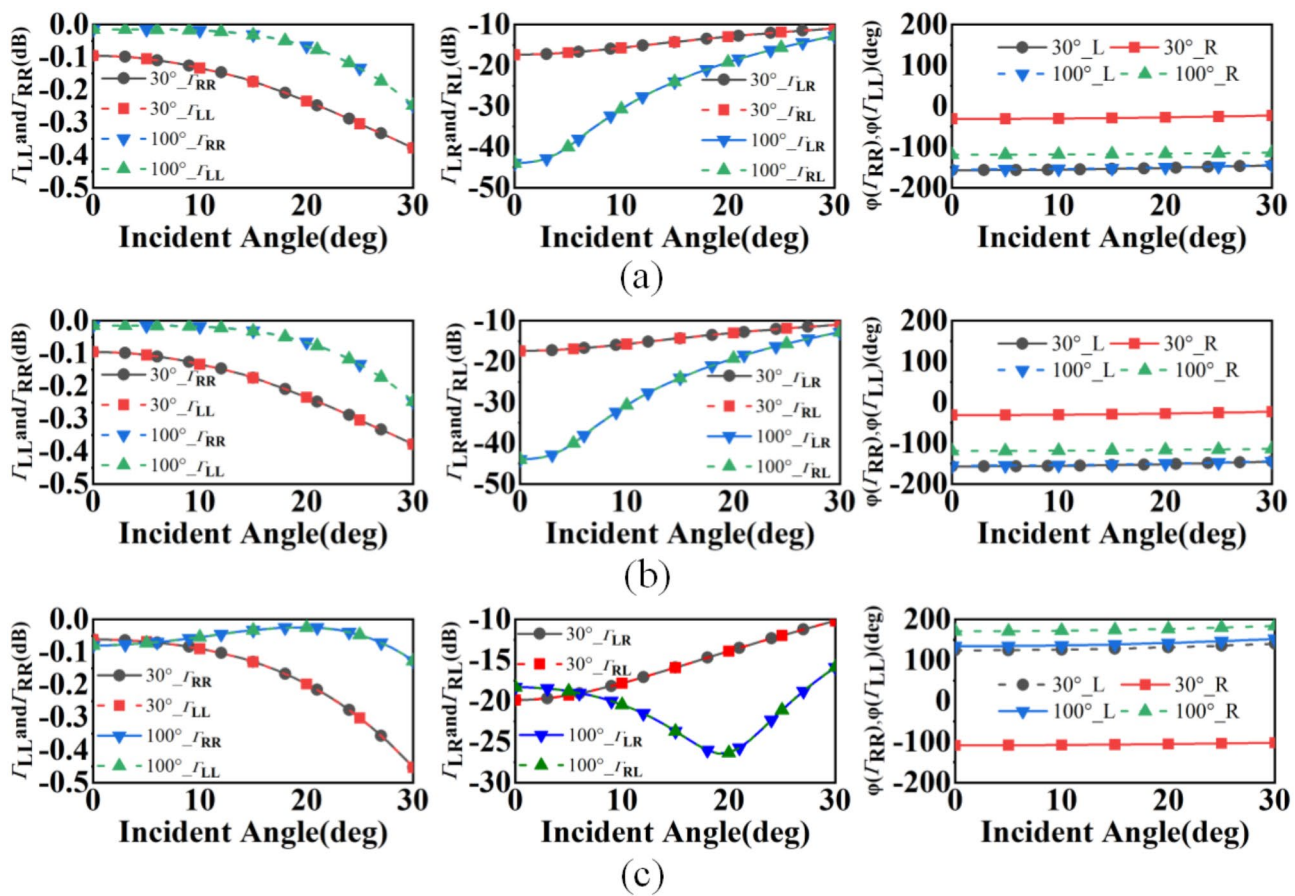


**Fig. 7.** Reflected coefficients and reflected phase of the co-polarized wave with incident angle degrees from 0° to 30° at (a) 10 GHz, (b) 11.725 GHz, (c) 15 GHz obtained by simulation.

the radiation is directed to the desired angle of  $(\phi L, \theta L) = (90^\circ, 20^\circ)$ . The gain can reach 29.1 dB with the maximum AE of 47%. The RHCP beam is directed to the desired angle of  $(\phi R, \theta R) = (-90^\circ, -20^\circ)$ . The gain is 29.22 dB and the AE is 48.3%. Compared with the existing similar work, the proposed dual-CP RA has the advantages of broad bandwidth, lower profile and higher AE.

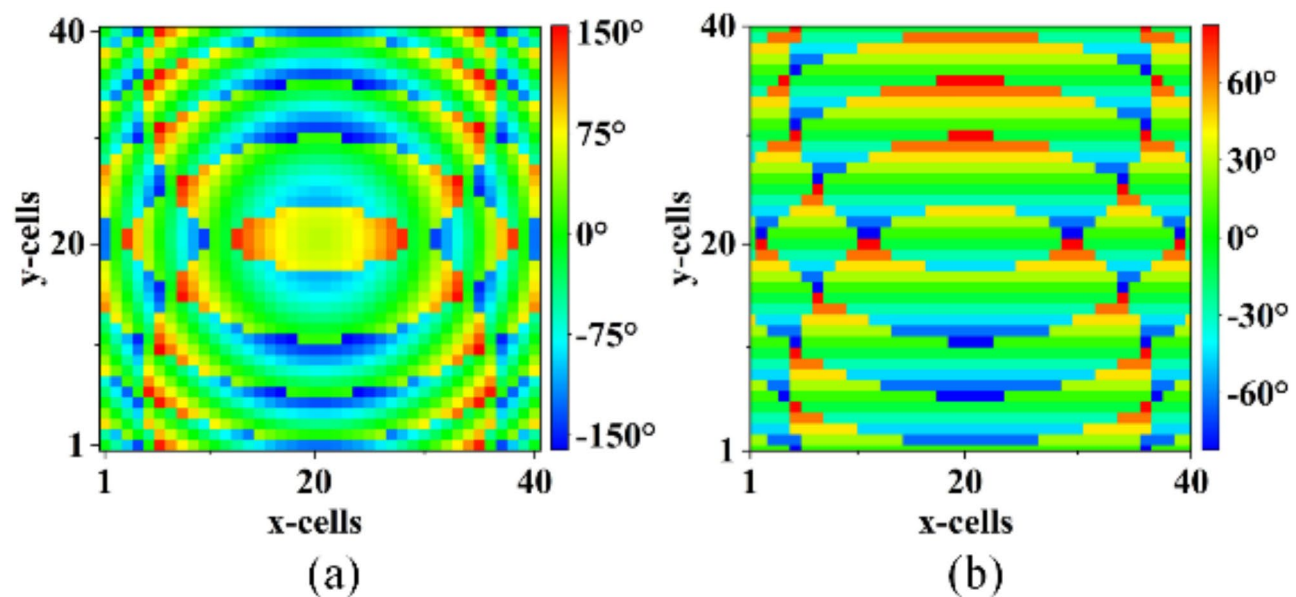


Fig. 8. Calculate results of (a) DP and (b) rotation angle distribution of dual-CP RA cells.

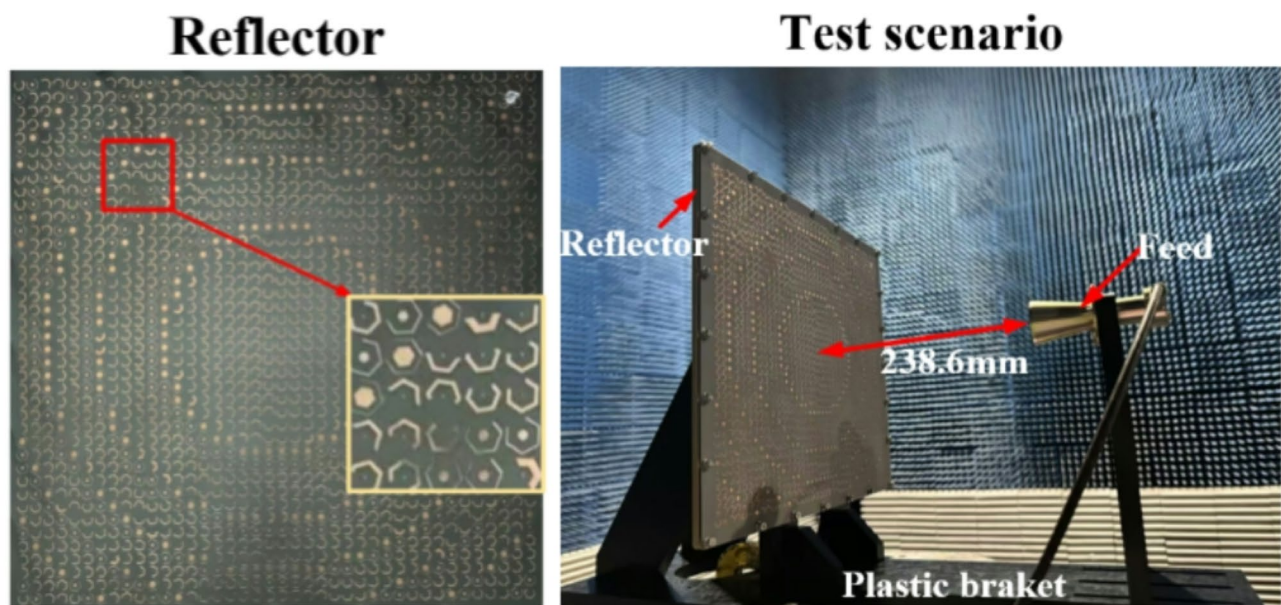
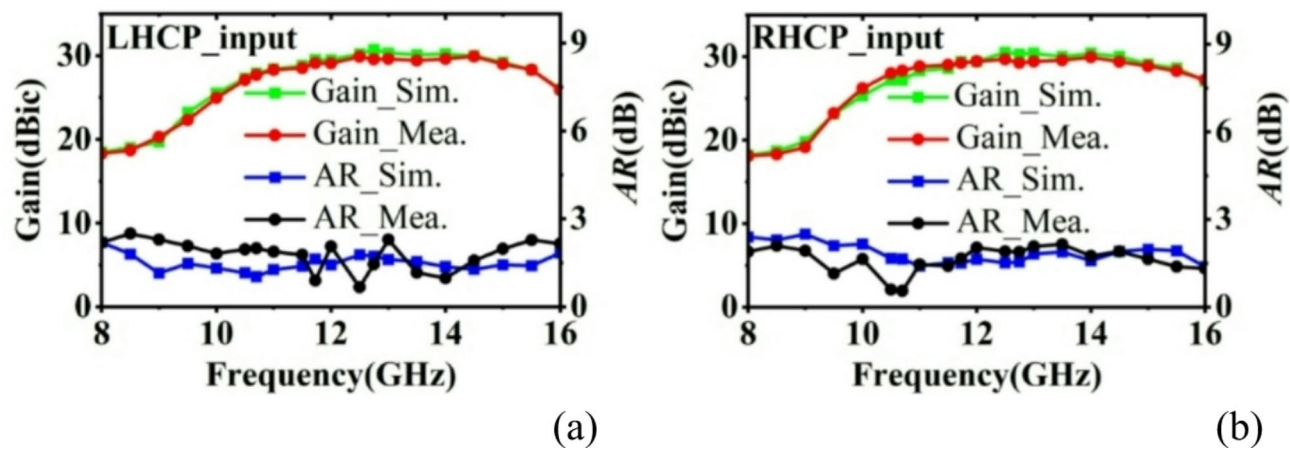
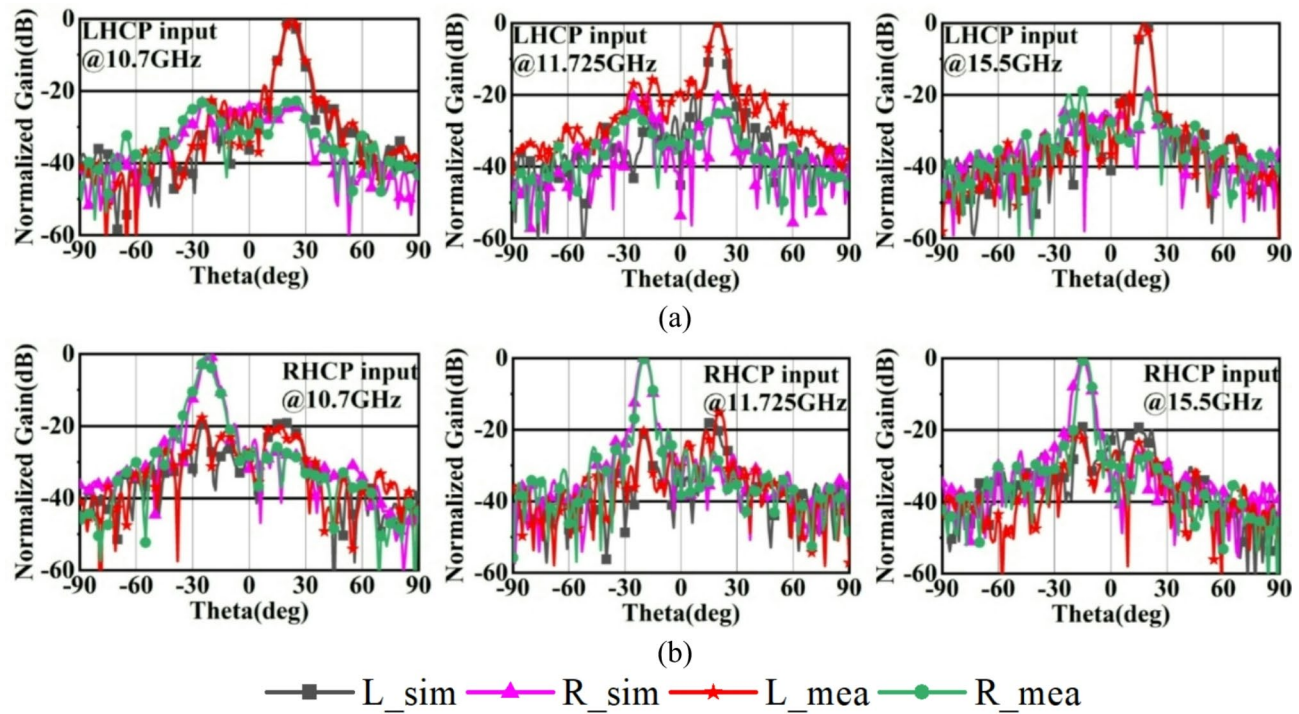


Fig. 9. The graph of the proposed dual-CP RA.



**Fig. 10.** Measured peak gain and AR of the dual-CP PRA fed by (a) LHCP horn and (b) RHCP horn.



**Fig. 11.** Measured radiation pattern of the dual-CP RA, (a) LHCP, (b) RHCP.

Ref.	Profile (mm)	Cells BW*	The number of cells	Aperture size (center frequency)	Function layers	AE (%)	Gain (dBi)	1 dB gain BW (%)	Technique
5	35.24/0.98 $\lambda_0$	–	97	7.3 $\lambda$	2	23.3	21	7	Multi-layer reflector
6	12.75/0.87 $\lambda_0$	~20%	4240	13.2 $\lambda$ *19.9 $\lambda$	3	22.6	27.5	5	LP RA and polarizer
7	1.73/0.11 $\lambda_0$	–	625	11.8 $\lambda$	3	66	29.5	7.6	BP and DP
8	2.95/0.29 $\lambda_0$	15.5%	688	15.9 $\lambda$	2	28	28	15	BP and DP
9	1.6/0.16 $\lambda_0$	~40%	904	15.6 $\lambda$	1	43	30	30	BP and DP
10	1.8/0.18 $\lambda_0$	64.3%	1013	16.5 $\lambda$	1	44.7/45.7	30.8/30.9	31.3/32.8	BP and DP
11	2.5/0.13 $\lambda_0$	–	1681	11.3 $\lambda$	1	53/54	29.5/29.6	25.1/25.3	BP and DP
12	3.51/0.23 $\lambda_0$	–	2128	26 $\lambda$	1	52.7/51.6	35.5/35.4	10.5/10	BP and DP
13	2.5/0.2 $\lambda_0$	–	2500	11.5 $\lambda$	1	64.9	29.6	17.1	DP
14	1.14/0.09 $\lambda_0$	–	324	8.4 $\lambda$	1	28.8	24.1/24	18.4/18.7	BP and DP
This work	3.1/0.12 $\lambda_0$	55.3%	1600	11.7 $\lambda$	1	47/48.3	29.1/29.2	37.4/37	BP and DP

**Table 2.** Comparisons with other dual-CP RAs. \*Cells BW: the cell's—10 dB Cross Polarization BW.

## Data availability

All data generated or analysed during this study are included in this published article.

Received: 27 December 2024; Accepted: 4 March 2025

Published online: 13 March 2025

## References

- Deng, R. Y., Yang, F., Xu, S. H. & Li, M. K. An FSS-Backed 20/30-GHz dual-band circularly polarized reflectarray with suppressed mutual coupling and enhanced performance. *IEEE Trans. Antennas Propag.* **65** (2), 926–931 (2017).
- Shamsaei Malfajani, R., Abbasi, B. & Arand Dual-band orthogonally polarized single-layer reflectarray antenna. *IEEE Trans. Antennas Propag.* **65** (11), 6145–6150 (2017).
- Xue, F., Wang, H. J., Yi, M., Liu, G. & Dong, X. C. Design of a broadband single-layer linearly polarized reflectarray using four-arm spiral elements. *IEEE Antennas Wirel. Propag. Lett.* **16**, 696–699 (2016).
- Mener, S., Gillard, R., Sauleau, R., Cheymol, C. & Potier, P. Design and characterization of a CPSS-based unit-cell for circularly polarized reflectarray applications. *IEEE Trans. Antennas Propag.* **61** (4), 2313–2318 (2013).
- Mener, S., Gillard, R., Sauleau, R., Bellion, A. & Potier, P. Dual circularly polarized reflectarray with independent control of polarizations. *IEEE Trans. Antennas Propag.* **63** (4), 1877–1881 (2015).
- Geaney, C. S., Hosseini, M. & Hum, S. V. Reflectarray antennas for independent dual linear and circular polarization control. *IEEE Trans. Antennas Propag.* **67** (9), 5908–5918 (2019).
- Florencio, R., Encinar, J. A., Boix, R. R., Barba, M. & Toso, G. Flat reflectarray that generates adjacent beams by discriminating in dual circular polarization. *IEEE Trans. Antennas Propag.* **67** (6), 3733–3742 (2019).
- Jiang, Z. H., Yue, T. & Hong, W. Low-profile and wideband dualcircularly polarized reflect-arrays based on rotated metal-backed dualpolarized aperture-coupled patch elements. *IEEE Trans. Antennas Propag.* **68** (3), 2108–2117 (2020).
- Jiang, Z. H., Zhang, Y. & Hong, W. Anisotropic impedance surface enabled low-profile broadband dual- circularly polarized multibeam reflectarrays for Ka-band applications. *IEEE Trans. Antennas Propag.* **68** (8), 6441–6446 (2020).
- Dai, X. W., Zhang, Y. H., Yu, W., Liu, L. & Luo, G. Q. A broadband low-profile dual-circularly polarized reflect-array based on a single-layer microstrip patch for Ka-band application. *IEEE Trans. Antennas Propag.* **71** (6), 4932–4940 (2023).
- Guo, W. L. et al. Broadband spin-decoupled metasurface for dual-circularly polarized reflector antenna design. *IEEE Trans. Antennas Propag.* **68** (5), 3534–3543 (2020).
- Zhang, X., Yang, F., Xu, S. & Li, M. Single-layer reflectarray antenna with independent dual-CP beam control. *IEEE Antennas Wirel. Propag. Lett.* **19** (4), 532–536 (2020).
- Xu, H. X. et al. Polarization-insensitive Metalens and its applications to reflectarrays with polarization diversity. *IEEE Trans. Antennas Propag.* **70** (3), 1895–1905 (2022).
- Fang, C. et al. Dual-circularly polarized reflectarray based on polarization selectivity of single-fed CP antenna element. *IEEE Trans. Antennas Propag.*, Early Access Article (2024).
- Jiang, Z. H. & Kang, L. W. H and D. H. Werner. Highly efficient broadband multiplexed millimeter-wave vortices from metasurface-enabled transmit-arrays of subwavelength thickness. *Phys. Rev. Appl.* **9** (6) (2018).
- Devlin, R. C., Ambrosio, A., Rubin, N. A., Mueller, J. P. B. & Capasso, F. Arbitrary spin-to-orbital angular momentum conversion of light. *Science* **358** (6365), 896–901 (2017).
- Encinar, J. A. Design of two-layer printed reflectarrays using patches of variable size. *IEEE Trans. Antennas Propag.* **49** (10), 1403–1410 (2001).

## Acknowledgements

This work was supported by the Key Research and Development Program of Shaanxi under Grant 2024GX-ZD-CYL-01-29 and in part by the Science and Technology Project of Xi'an City under Grant 24KPZT0010.

## Author contributions

M.Y.T and R.Y.H. wrote the main manuscript text and M.Y.T prepared Figs. 1, 2, 3, 4, 5, 6, 7, 8, 9 and 10; Table 1, and 2. All authors reviewed the manuscript.

## Declarations

### Competing interests

The authors declare no competing interests.

### Additional information

**Correspondence** and requests for materials should be addressed to Y.R.

**Reprints and permissions information** is available at [www.nature.com/reprints](http://www.nature.com/reprints).

**Publisher's note** Springer Nature remains neutral with regard to jurisdictional claims in published maps and institutional affiliations.

**Open Access** This article is licensed under a Creative Commons Attribution-NonCommercial-NoDerivatives 4.0 International License, which permits any non-commercial use, sharing, distribution and reproduction in any medium or format, as long as you give appropriate credit to the original author(s) and the source, provide a link to the Creative Commons licence, and indicate if you modified the licensed material. You do not have permission under this licence to share adapted material derived from this article or parts of it. The images or other third party material in this article are included in the article's Creative Commons licence, unless indicated otherwise in a credit line to the material. If material is not included in the article's Creative Commons licence and your intended use is not permitted by statutory regulation or exceeds the permitted use, you will need to obtain permission directly from the copyright holder. To view a copy of this licence, visit <http://creativecommons.org/licenses/by-nc-nd/4.0/>.

© The Author(s) 2025